THE JOURNAL OF PHYSICAL CHEMISTRY B
A JOURNAL OF THE AMERICAN CHEMICAL SOCIETY

pubs.acs.org/JPCB

Article

Correlation between Charge Transport and Base Excision Repair in the MutY–DNA Glycosylase

Ruijie D. Teo,* Xiaochen Du, Héctor Luis Torres Vera, Agostino Migliore, and David N. Beratan*

Cite This: *J. Phys. Chem. B* 2021, 125, 17–23

Read Online

ACCESS | Metrics & More | Article Recommendations | Supporting Information

ABSTRACT: Experimental evidence suggests that DNA-mediated redox signaling between high-potential $[Fe_4S_4]$ proteins is relevant to DNA replication and repair processes, and protein-mediated charge transfer (CT) between $[Fe_4S_4]$ clusters and nucleic acids is a fundamental process of the signaling and repair mechanisms. We analyzed the dominant CT pathways in the base excision repair glycosylase MutY using molecular dynamics simulations and hole hopping pathway analysis. We find that the adenine nucleobase of the mismatched A·oxoG DNA base pair facilitates $[Fe_4S_4]$–DNA CT prior to adenine excision by MutY. We also find that the R153L mutation in MutY (linked to colorectal adenomatous polyposis) influences the dominant [Fe4S4]–DNA CT pathways and appreciably decreases their effective CT rates.

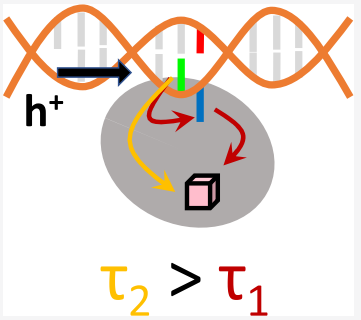

1. INTRODUCTION

Charge transfer (CT) processes are ubiquitous in cell biology, where they are used both to drive reactions[1] and to convey signals.[2] In protein–nucleic acid complexes, the protein medium can support CT between a redox cofactor and the nucleic acid duplex for purposes that might range from detection/repair of DNA defects[2−5] to signaling between proteins for coordination of their activity.[6−9] In these contexts, the π-stacking of DNA nucleobases allows the charge to propagate over distances up to a nanometer scale.[10] CT also governs redox signaling that occurs in response to changes in reactive oxygen species or reactive nitrogen species levels in the cellular system.[11,12] Redox signaling processes are paramount in the regulation of major cellular pathways. Structural changes in proteins and/or DNA can alter the CT pathways, dysregulate cellular signaling, and thus result in the over proliferation of cells, contributing to human diseases like cancer.[2,13]

DNA-mediated CT between high-potential $[Fe_4S_4]^{2+/3+}$ proteins is hypothesized as a means of coordinating DNA replication and repair.[2,3] High-potential $[Fe_4S_4]$ clusters can play a structural role, and experiments[4,6] suggest that these clusters are involved in the regulation of the enzyme activity.[14,15] Alternation between the reduced and oxidized states of a high-potential $[Fe_4S_4]$ cofactor via DNA-mediated CT may synchronize the binding and unbinding events required for the functioning of $[Fe_4S_4]$ proteins involved in DNA repair and replication. These events are believed to be governed to a great extent by electrostatic interactions in which a protein containing a $[Fe_4S_4]^{3+}$ cluster is electrostatically more strongly attracted and binds more tightly to the negatively charged DNA backbone than a $[Fe_4S_4]^{2+}$-containing protein.[16] Anaerobic microscale thermophoresis indicates that the DNA–protein binding affinity increases by 550-fold in the presence of $[Fe_4S_4]^{3+}$.[16] This increased DNA binding also induces a shift of the $[Fe_4S_4]^{2+/3+}$ redox couple to ca. +80 mV versus NHE (normal hydrogen electrode).[7,17,18]

The redox signaling between two $[Fe_4S_4]$ proteins linked by a DNA duplex requires DNA-mediated CT and protein-mediated CT between the iron–sulfur clusters and the duplex. Recent studies report the unidirectional nature of CT between $[Fe_4S_4]$ clusters and nucleic acid duplexes[19] and the general feasibility of CT through a protein on μs-to-ms timescales using a multistep hopping mechanism.[19,20] Moreover, mutation effects on the preferential charge hopping routes through proteins were described.[20] These findings motivate the study of the functional role of CT in protein–nucleic acid complexes, with the aim of providing insights into possible connections between mutation and health consequences.

Within the above context, base excision repair (BER) glycosylases are a class of $[Fe_4S_4]^{2+/3+}$-containing proteins whose interface with DNA offers a rich medium for functional CT, including intra-DNA CT as well as direct and protein-mediated CT between the DNA and the $[Fe_4S_4]$ cluster. Electrochemistry and atomic force microscopy experiments indicate that the DNA–$[Fe_4S_4]$ CT in these proteins is facilitated by the positioning of the enzyme in proximity to the base-pair mismatch.[4,18,21,22] One of the most studied BER

Received: September 21, 2020
Revised: November 22, 2020
Published: December 29, 2020

https://dx.doi.org/10.1021/acs.jpcb.0c08598
J. Phys. Chem. B 2021, 125, 17–23

enzymes is MutY,[23−25] which excises an adenine residue (DA18 shown in Figure 1) from a mismatched A·oxoG base

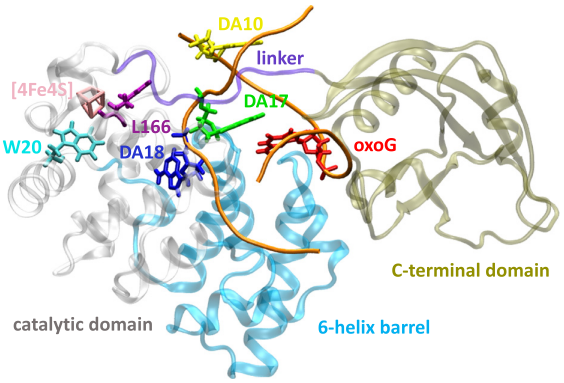

Figure 1. Structure of the MutY−DNA complex (PDB file 1RRQ[23]) containing the A·oxoG mismatched pair. The sugar−phosphate backbone of DNA is colored in orange.

pair. This base mismatch arises in the presence of oxidative stress, when a guanine nucleobase is oxidized and a DNA polymerase inserts an adenine rather than a cytosine on the complementary strand. The excision of adenine by MutY produces an abasic site and a free adenine nucleobase. Repair polymerases and MutM eventually convert the abasic site and oxoG into the correct C·G base pair.

In the MutY−DNA complex (PDB file 1RRQ; see Figure 1),[23] the $[Fe_4S_4]$ cluster is located in the catalytic domain, while the DNA is sandwiched between the catalytic and C-terminal domains. The adenine nucleobase of the A·oxoG pair (i.e., DA18, Figure 1) extrudes from the DNA double helix and extends into the catalytic domain. This extrusion is also observed in other DNA glycosylase complexes that repair single-base lesions.[23] The nucleobase extrusion is attributed to the transition of the N-glycosidic bond of oxoG from a *syn* conformation to an *anti* conformation when the DNA binds to MutY (Figure 1).[23] In the *anti* conformation, oxoG clashes sterically with DA18, thus promoting its extrusion. As DA18 fails to π-stack with other nucleobases and extends into the protein, DA18 could serve as a bridge site in the DNA−$[Fe_4S_4]$ CT pathway, rather than as a terminal donor/acceptor site. Another adenine nucleobase (DA17) in the base pair next to A·oxoG (Figures 1 and 2) seems to be a good nucleobase candidate for oxidizing the $[Fe_4S_4]^{2+}$ cluster because of the DA17−cluster edge-to-edge distance of 17.7 Å. The next shortest distance between the cluster and other nucleobases in the double-stranded DNA is 20.0 Å (DA10−cluster).

While the feasibility of $[Fe_4S_4]$−DNA CT in the MutY complex was demonstrated experimentally,[24,25] in this study, we probe the mechanistic characteristics of this CT process using molecular dynamics (MD) simulations and an improved version of the EHPath code that identifies charge hopping pathways and assesses their corresponding transit times.[19] We streamlined the prior hopping pathway search code[19] to enable CT analysis of multiple MD trajectories using either a local computer or a computer cluster. The CT analysis described here assumes that signaling/repair by MutY is triggered by transport of a hole from an initially oxidized DNA molecule (i.e., a structure under oxidative stress) to the $[Fe_4S_4]$ cluster. We found that the DA17 nucleobase is the most likely hole donor based on constraints of thermodynamics and distances

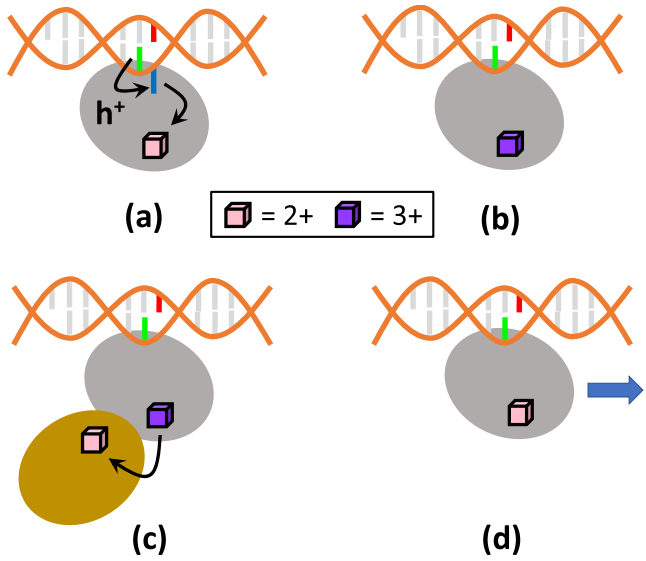

Figure 2. Proposed mechanism for the excision of mismatched DNA bases by MutY. The mechanism is substantially based on CT between the DNA and the $[Fe_4S_4]$ cluster and proceeds through the following steps: (a) the oxidized nucleobase DA17 transfers the hole to $[Fe_4S_4]^{2+}$ via a hopping pathway involving DA18, thus leading to $[Fe_4S_4]^{3+}$. (b) The DNA-bound MutY excises DA18, as part of the DNA repair process. (c) CT between $[Fe_4S_4]^{3+}$ in MutY and $[Fe_4S_4]^{2+}$ in a partner repair protein may reduce $[Fe_4S_4]^{3+}$ to $[Fe_4S_4]^{2+}$. (d) The absence of DA18 prevents the cluster from being easily reoxidized by a nucleobase. The $[Fe_4S_4]^{2+}$-containing MutY is thus able to slide along the DNA and search for further base mismatches. Color code: MutY (gray), oxoG (red), DA17 (green), DA18 (blue), and $[Fe_4S_4]$ partner protein (gold).

that determine the CT kinetic timescales.[26] It is thought that the change in the $[Fe_4S_4]$ cluster charge (after oxidation) can oxidize a partner repair protein, which in turn allows the now-reduced MutY to slide along the DNA and identify other base mismatches.[4,24,25] Here, we propose a mechanistic interpretation of BER by MutY−DNA based on the CT between the $[Fe_4S_4]$ cluster and the DNA at the MutY−DNA interface. The proposed mechanism unifies the knowledge gained from the CT hopping pathway analysis with the current understanding of the DNA repair process. Furthermore, we describe the influence of the R153L mutation in the MutY protein (which is associated with colorectal adenomatous polyposis[27]) on the pathways and transit times for CT between the $[Fe_4S_4]$ cluster contained in the protein and the bound DNA.

2. METHODS

2.1. System Modeling. The structure of the MutY−DNA complex was obtained from the PDB file 1RRQ.[23] The missing residues (i.e., 230−233 and 288−291) were added using the MODELLER program.[28] Since the crystal structure contains several mutations (D144N, P164C, F347S, and K357E) that helped to stabilize the A·oxoG complex and amplify its expression, these mutated residues were replaced with the original residues using PyMOL, while our attention was focused on the effect of the R153L mutation.[29] Moreover, while a study by Verdine et al.[30] indicated that the D144N mutation may prevent full engagement of DA18 with MutY, we decided to use PDB 1RRQ as it contains unmodified DNA (versus the fluorinated DNA in PDB 3G0Q[30]). The resulting structure was used in the MD simulations.

https://dx.doi.org/10.1021/acs.jpcb.0c08598
J. Phys. Chem. B 2021, 125, 17−23

2.2. MD Simulations. MD simulations (using NAMD 2.11[31]) of the wild-type (WT) MutY–DNA complex were performed using the A_{2+} and A_{3+} force fields (FFs) reported in ref.[20] for the $[Fe_4S_4]^{2+}$ and $[Fe_4S_4]^{3+}$ clusters. The $[Fe_4S_4]$ cluster in MutY changes from its 2+ oxidation state to the 3+ state as it receives a hole from an oxidized nucleobase. As in other protein–DNA complexes,[20] the timescale for CT between the nucleobase and $[Fe_4S_4]$ is much slower than the accessible simulation timescale (vide infra). Ideally, the FFs used in the MD simulation should be updated as the charge hops from the hole donor in the DNA to the iron–sulfur cluster. As we recently observed,[20] a more practical MD approach is to analyze the dynamics of the protein–DNA complex using both the A_{2+} and the A_{3+} FFs,[20] while reactive FFs that allow for bond breaking and formation were not considered for the purposes of this study that focuses on electron–hole transfer.[32] The FF parameters for the oxoG moiety were obtained from ref.[33] AMBER FFs ff14SB[34] and ff99-bsc0[35,36] FFs were used to describe the rest of the protein and DNA. We also mutated Arg153 to Leu and simulated the mutated MutY–DNA complex using the A_{2+} and A_{3+} FFs. The R153L mutation in the *Bacillus stearothermophilus* protein obtained from the 1RRQ[23] PDB file corresponds to the R231L mutation that in the human homolog (hMYH) is associated with colorectal adenomatous polyposis.[27]

For each simulation, Na^+ ions were added to neutralize the biomolecular system and TIP3P water was used to solvate the protein–DNA complex, extending 10 Å on each side of the unit cell. The resulting unit cell had a size of $72 \times 79 \times 101$ Å^3. We used the SHAKE algorithm to constrain the interatomic distances (H–O and H–H) in the water molecules.[37] The electrostatic interaction energy was calculated every 2 MD time steps using the particle mesh Ewald summation method,[38] with a grid spacing of 1 Å and a scaling factor of 0.833333 for 1–4 interactions. For nonbonded atomic pairs, the cutoff distance for the periodic calculation of their interaction energy was set to 14 Å, and the van der Waals interactions were truncated at 12 Å.

We conducted 8×10^4 steps of energy minimization and 150 ps of solvent equilibration at 298 K (namely, the crystallization temperature of the 1RRQ structure) using a Langevin thermostat with a damping coefficient of 1.0 ps^{-1}. During this equilibration, the coordinates of the protein–nucleic acid complex were fixed. We next carried out another 125 ps of equilibration at 298 K, releasing all atoms in the protein–DNA complex. This equilibration was followed by another 1.5 ns of equilibration at a constant temperature (298 K) and pressure (1 atm), using a Nosé–Hoover Langevin piston pressure control[39,40] with a piston period of 100 fs, a damping coefficient of 2.0 ps^{-1}, and a barostat damping time of 50 fs. Each MD production run lasted 60 ns, with a time step of 0.5 fs. The RMSDs (root-mean-square deviations) along the MD trajectories are shown in Figure S1. Snapshots within the 10–60 ns time window were extracted every 0.5 ns to analyze the CT pathways between the $[Fe_4S_4]$ cluster and DNA using EHPath_multirun.py (see github.com/etransfer/EHPath).

2.3. Kinetic Modeling. The CT rate constant k for each CT step was calculated using a nonadiabatic CT rate expression with Marcus' high-temperature Franck–Condon factor[41]

$$k = \frac{2\pi}{\hbar}\langle V^2\rangle \frac{1}{\sqrt{4\pi\lambda k_B T}} \exp\left[\frac{-(\Delta G^\circ + \lambda)^2}{4\lambda k_B T}\right] \quad (1)$$

In eq 1, V is the electronic coupling between the initial and final electronic states, λ is the reorganization energy, ΔG° is the reaction free energy, and T is the temperature (in our study, T = 298 K). In the EHPath (and the updated EHPath_multirun.py) code,[19] V is obtained from the charge donor–acceptor distance using a square-tunneling barrier model, λ is obtained using Marcus' two-sphere model[41−43] and ΔG° is approximated as the difference in the donor and acceptor redox potentials (see refs. 19 and 42 for further details regarding the CT parameters).

Depending on the donor–acceptor distance in a given molecular conformation, the excess charge can either tunnel directly from the donor to the terminal acceptor site or it can follow a multistep hopping pathway. Both CT processes are consistently described by birth-and-death kinetic models.[44−46] As described previously, the final charge acceptor either behaves as an absorber[42] or is in contact with a charge drain,[8] and the overall mean residence time τ of the charge in a path (the charge transit time) can be written in a compact form[8] (a different derivation for the kinetic model with an absorber is reported in ref.[45])

$$\tau = \sum_{n=0}^{N-1} \frac{1}{k_{n\to n+1}} \left(\sum_{j=0}^{N-n-1} \prod_{i=n+1}^{N-j} \frac{k_{i\to i-1}}{k_{i\to i+1}} + 1 \right) + \frac{1}{k_{N\to N+1}} \quad (2)$$

This transit time is implemented in EHPath_multirun.py.[19] N is the total number of hopping sites in the pathway and $k_{n\to n\pm1}$ is the rate constant for CT between the nearest-neighbor redox sites n and $n \pm 1$. $n = 0$ denotes the initial charge donor, $n = 1$ to N denotes the bridge sites, and site $n = N + 1$ is the terminal charge acceptor. The forward and reverse CT rate constants obtained using eq 1 for each nearest-neighbor hop were used in eq 2. In our kinetic analysis, only the forward rate was considered for the CT step between site $n = N$ and the terminal acceptor site. That is, the final CT step is irreversible. This irreversibility models rapid scavenging of the excess charge by redox agents in the cell[42] or trapping of the charge on the terminal acceptor.[20,42,43]

EHPath_multirun calculates τ for electron or hole transport pathways. With EHPath_multirun, one can either treat $[Fe_4S_4]^{2+}$ as the electron donor and a nucleobase as the electron acceptor, or treat a nucleobase as the hole donor and $[Fe_4S_4]^{2+}$ as the hole acceptor. These two options (with their different approximations in describing the individual CT steps and their different boundary conditions[20]) define kinetic models 1 and 2, respectively, in the following analysis. We investigated both electron and hole hopping pathways between $[Fe_4S_4]$ and DNA using these two models (Section 3).

3. RESULTS AND DISCUSSION

3.1. Charge Transport in the MutY–DNA Complex. With both choices of kinetic models and FFs, we find that the dominant CT pathway between $[Fe_4S_4]$ and DNA (namely, the fastest hole hopping route in most of the selected system's snapshots) contains DA18 as a bridge site and DA17 as the hole donor in kinetic model 1 or as the electron acceptor in kinetic model 2 (see Table 1). Although DA17 could donate the hole to oxoG since the reduction potential of oxoG is 0.74

https://dx.doi.org/10.1021/acs.jpcb.0c08598
J. Phys. Chem. B 2021, 125, 17−23

Table 1. Strongest CT Pathways Computed for the WT MutY−DNA Complex, Using A_{2+} and A_{3+} FFs To Describe the Iron−Sulfur Cluster in the MD Simulation

FF	kinetic model	CT pathways	%
A_{2+}	1	$[Fe_4S_4]$−DA18−DA17	80.2
		$[Fe_4S_4]$−W20−DA18−DA17	19.8
	2	DA17−DA18−$[Fe_4S_4]$	79.2
		DA17−DA18−W20−$[Fe_4S_4]$	19.8
		DA17−$[Fe_4S_4]$	1.0
A_{3+}	1	$[Fe_4S_4]$−DA18−DA17	95.0
		$[Fe_4S_4]$−W20−DA18−DA17	5.0
	2	DA17−DA18−$[Fe_4S_4]$	95.0
		DA17−DA18−W20−$[Fe_4S_4]$	5.0

V versus NHE,[47] this hole can easily be "trapped" at oxoG due to the higher reduction potentials of the adjacent purines. In the presence of an oxidative environment, it is very likely that another hole will arrive at DA17 through DNA hole transfer and proceed to other bridge sites such as DA18. In fact, all pathways (with the exception of 1% of the pathways for kinetic model 2 and A_{2+}) contain DA18, and all hole (electron) hopping routes begin (end) at DA17. W20 is found to serve as a bridge hopping site in some of the CT pathways (Table 1), due to its proximity to $[Fe_4S_4]$ and DA18 (Figure 1 and Tables S1, S2), and to its contribution to a favorable energy landscape for CT. In fact, the oxidation potential of the Trp residue lies between the $[Fe_4S_4]$ and adenine oxidation potentials.[42] We note that a higher percentage of CT pathways involves W20 when the A_{2+} FF is used in the MD simulation (19.8%) than when A_{3+} is used (5.0%) (Table 1). Since the CT rate constant k in eq 1 drops exponentially with the donor−acceptor distance (due to the electronic coupling factor), and the reorganization energy grows with distance, this difference in the W20 contribution to the CT may be attributed to the larger W20−DA18 distance (15.8 Å, see Table S1) in the A_{3+} MD simulation compared to the A_{2+} simulation (15.0 Å). This increased distance produces a smaller W20−DA18 CT rate, so that other CT pathways that do not involve W20 are kinetically more favorable. Aside from this difference, the same qualitative picture emerges from the A_{2+} and A_{3+} simulations. In particular, the CT analysis of both MD simulations indicates that DA18 is an essential hopping site for CT between the DNA and the iron−sulfur cluster.

The $[Fe_4S_4]$-to-DA17 mean transit time averaged over the MD snapshots, $\langle\tau\rangle$, ranges from 0.7 to 1.7 ms (Table 2), which is within the millisecond (1−4 ms[48]) half-life of adenine radicals. Therefore, CT to the iron−sulfur cluster provides a viable route for the reduction of adenine.

To further analyze the role of DA18 in the CT chain, we computed the CT pathways between $[Fe_4S_4]$ and DA17 excluding DA18 as one of the possible bridge sites. Using both kinetic models 1 and 2 and both A_{2+} and A_{3+} FFs, we found that the average charge travel time $\langle\tau\rangle$ increases by about an order of magnitude ($\langle\tau\rangle$ is in the range 11.2−13.6 ms; see Table 3) compared to the value that is obtained including DA17 in the hopping pathway analysis. The comparison of the charge transit times provided in Tables 2 and 3 with the adenine radical half-life (1−4 ms) indicates that the DA18 base to be excised serves as an essential bridge for sufficiently rapid oxidation of the $[Fe_4S_4]^{2+}$ cluster by the DA17 radical cation, prior to DA17 reduction by other redox agents in the cell.

Table 2. Average Mean Residence Times $\langle\tau\rangle$ (in ms) Computed for the WT MutY−DNA Complex Using the Selected MD Snapshots

FF	$\langle\tau\rangle_{\text{kinetic model 1}}$	$\langle\tau\rangle_{\text{kinetic model 2}}$
A_{2+}	1.3 ± 1.6	1.7 ± 1.9
A_{3+}	0.7 ± 0.3	0.9 ± 0.4

Table 3. Average Mean Residence Times $\langle\tau\rangle$ (in ms) for the WT MutY−DNA Complex Excluding DA18 from the CT Pathways

FF	$\langle\tau\rangle_{\text{kinetic model 1}}$	$\langle\tau\rangle_{\text{kinetic model 2}}$
A_{2+}	11 ± 14	14 ± 16
A_{3+}	11 ± 10	11 ± 10

The extrusion of DA18, upon DNA recognition by MutY, appears to optimally position DA18 both to serve as a key charge hopping site for DNA reduction/$[Fe_4S_4]$ cluster oxidation on a millisecond timescale and also to enable the base excision by the catalytic domain. The computed difference in $\langle\tau\rangle$ with and without DA18 suggests a possible mechanism for nucleobase excision preceding DNA repair. As MutY is near the mismatched A·oxoG pair, the $[Fe_4S_4]^{2+}$ cluster of MutY is oxidized to the 3+ state by DA17, via DA18 (Figure 2a). The oxidation of the iron−sulfur cluster is expected to strengthen the MutY−DNA binding,[7] thus favoring the excision of the mismatched DA18 nucleobase by MutY's catalytic domain (Figure 2b). Then, the $[Fe_4S_4]^{3+}$ cluster might be reduced to $[Fe_4S_4]^{2+}$ by a partner protein (e.g., a nearby $[Fe_4S_4]$-containing repair polymerase that is then responsible for inserting the correct nucleobase at the excision site[3,49]) (Figure 2c). The switch in the $[Fe_4S_4]$ redox state would weaken the MutY−DNA binding and thus allow MutY to slide along the DNA duplex and continue its search for other base-pair mismatches (Figure 2d). Furthermore, since the timescale for an initially oxidized nucleobase to transfer the hole to the $[Fe_4S_4]$ cluster is larger without DA18, the excision of DA18 by MutY also discourages another hole on DNA from reoxidizing the $[Fe_4S_4]$ cluster (which would hinder the protein sliding) until the next DNA mismatch is encountered. In vitro experiments would be necessary to test the proposed mechanism since it involves the coordination between MutY and its partner protein. In particular, future experiments should verify that the reduction of the $[Fe_4S_4]^{3+}$ cluster of MutY does not occur before the excision of DA18.

3.2. Mutation Effect on MutY−DNA Charge Transport. The R153L mutation (associated with colorectal adenomatous polyposis[27]) influences the occurrences and transit times of the $[Fe_4S_4]$−DNA CT pathways. However, the computed mutation effects depend somewhat on the FF used for the $[Fe_4S_4]$ cluster.

In the MD simulations of the mutated protein complex using the A_{2+} FF, the dominant CT route is either direct $[Fe_4S_4]$−DA17 tunneling (kinetic model 1) or DA17−DA18−W20−$[Fe_4S_4]$ (kinetic model 2) (see Table 4). In contrast, $[Fe_4S_4]$−DA18−DA17 (kinetic model 1), and conversely, DA17−DA18−$[Fe_4S_4]$ (kinetic model 2) were the dominant CT pathways found for the WT protein−DNA complex using the same A_{2+} FF (and indeed, also using the A_{3+} FF; see Table 1). These differences in CT pathways are consistent with the fact that the average $[Fe_4S_4]$−DA18 distance increases from 18.8 Å in the WT protein complex to 20.4 Å in the R153L protein

https://dx.doi.org/10.1021/acs.jpcb.0c08598
J. Phys. Chem. B 2021, 125, 17−23

Table 4. Distribution of CT Pathways Computed for the R153L MutY−DNA Complex, Using A_{2+} and A_{3+} FFs To Describe the Iron−Sulfur Cluster in the MD Simulation

FF	kinetic model	CT pathways	%
A_{2+}	1	$[Fe_4S_4]$−DA17	77.2
		$[Fe_4S_4]$−DA18−DA17	14.9
		$[Fe_4S_4]$−DA10	6.9
		$[Fe_4S_4]$−W20−DA18−DA17	1.0
	2	DA17−DA18−W20−$[Fe_4S_4]$	82.2
		DA17−DA18−$[Fe_4S_4]$	16.8
		DA17−$[Fe_4S_4]$	1.0
A_{3+}	1	$[Fe_4S_4]$−DA18−DA17	80.2
		$[Fe_4S_4]$−W20−DA18−DA17	19.8
	2	DA17−DA18−$[Fe_4S_4]$	80.2
		DA17−DA18−W20−$[Fe_4S_4]$	19.8

complex (Tables S1, S2), while the average $[Fe_4S_4]$−DA17 distance only experiences a modest increase from 22.0 to 22.2 Å upon mutation. The mutation also leads to the observation of direct CT between the cluster and DA10, which was not found in the WT complex. This observation is consistent with the decrease in the average $[Fe_4S_4]$−DA10 distance from 22.3 to 21.6 Å upon mutation (Table S2).

The MD simulation of the mutated system with the A_{3+} FF leads, instead, to the same dominant CT pathways as in the WT protein complex (compare the bottom panels in Tables 1 and 4). However, the occurrence frequencies and transit times for these pathways change appreciably upon protein mutation. The mutation increases the average distance between the initial charge donor and the final acceptor from 21.96 to 23.06 Å, with a consequent decrease in the electronic coupling. This change favors more frequent charge hopping through W20 compared to the WT system, and overall, decreases the CT speed (see Table 5). A decrease in the effective CT rate $(1/\tau)$ is consistently obtained from the MD simulations using the A_{2+} and A_{3+} FFs, despite the structural differences that emerge from the two MD simulations and related changes in the CT pathways. It is worth noting that the structural differences arising in the two MD simulations are relatively small, but they significantly affect the CT routes, primarily because of the exponential dependence of the electronic couplings on the donor−acceptor distances. Since the $[Fe_4S_4]$−DA17 and $[Fe_4S_4]$−DA18 distances are significantly larger than the DA17−DA18 distance in both the WT and R153L protein complexes, we expect that the A_{2+} reduced-cluster FF describes the CT system more realistically than the A_{3+} FF. However, this expectation is mitigated by the transient charge localization on the W20 residue (which is midway between the $[Fe_4S_4]$ cluster and the DNA) in the dominant CT pathways (see Section 2.2 and ref.[20]).

Table 5. Average Mean Residence Times $\langle\tau\rangle$ (ms) Computed for the R153L MutY−DNA Complex across the Selected MD Snapshots

FF	$\langle\tau\rangle_{\text{kinetic model 1}}$	$\langle\tau\rangle_{\text{kinetic model 2}}$
A_{2+}	2.0 ± 0.8	3.0 ± 2.3
A_{3+}	1.9 ± 1.3	2.3 ± 1.4

Irrespective of the computational approach used, we find that the $\langle\tau\rangle$ value for the WT protein−DNA system (Table 2) increases by approximately 1 ms upon R153L mutation (cf. Table 5). This increase in $\langle\tau\rangle$ should be considered cautiously because of the approximations in the simulations. Nonetheless, this increase may have important mechanistic implications if experimentally validated. To understand the implications, we note that the half-life of adenine radicals ranges from 1 to 4 ms in experiments.[48] Thus, if the half-life of the DA17 cation in the local DNA environment is 1 ms, for example, the predicted increase in $\langle\tau\rangle$ upon protein mutation makes CT to the $[Fe_4S_4]$ cluster noncompetitive with other mechanisms for DA17 reduction. In these circumstances, mutation would significantly limit cluster oxidation, thus preventing tight protein−DNA binding, favoring the continuous sliding of R153L MutY along the DNA and hampering the DA18 excision.

4. CONCLUSIONS

We studied functional CT at the interface between the $[Fe_4S_4]$-containing BER enzyme MutY and DNA using MD simulations and CT analysis with an enhanced version of our program[19] to search for CT hopping pathways on numerous structures derived from MD simulations (EHPath_multir-un.py).

After structural refinement and simulation of the protein−DNA complex from the PDB file 1RRQ,[23] we found that the hole transport occurs preferentially between the $[Fe_4S_4]$ cluster and the DA17 nucleobase, and that the mismatched DA18 base acts as a critical hole hopping site prior to its excision. DA18 reduces, by an order of magnitude, the time required for the iron−sulfur cluster oxidation, which strengthens the protein−DNA binding and favors the DA18 excision by the catalytic domain.

Our analysis indicates that the R153L mutation in MutY slows the rate of $[Fe_4S_4]^{2+}$ oxidation by the reduction of DA17. Therefore, in the mutated system, the DA17 radical cation can be more readily reduced by other competing processes in the cell. We argue that the decrease in the $[Fe_4S_4]^{2+}$ oxidation rate can be linked to a decreased ability of the R153L mutant to excise DA18, which may allow an interpretation of the relationship between the R153L mutation and colorectal adenomatous polyposis in terms of mutation effects on the functional CT at the protein−DNA interface.

Future experiments involving DNA-mediated electrochemical assays could examine possible changes in the DNA−$[Fe_4S_4]$ charge transit time by exploring different DNA sequences bound to MutY. As the function of MutY is to excise adenine from its mispaired oxoG partner, MutY positions its $[Fe_4S_4]$-containing catalytic domain in proximity to the A·oxoG base pair for eventual excision. This invariably increases the likelihood for DNA−$[Fe_4S_4]$ CT, which may unlikely alter the charge transit time significantly.

■ ASSOCIATED CONTENT

Supporting Information

The Supporting Information is available free of charge at https://pubs.acs.org/doi/10.1021/acs.jpcb.0c08598.

RMSDs of the (WT and mutant) MutY−DNA complexes during the MD production run and the center-to-center distances of the redox pairs obtained using the A_{3+} and A_{2+} FFs (PDF)

https://dx.doi.org/10.1021/acs.jpcb.0c08598
J. Phys. Chem. B 2021, 125, 17−23

AUTHOR INFORMATION

Corresponding Authors

Ruijie D. Teo − *Department of Chemistry, Duke University, Durham, North Carolina 27708, United States;* orcid.org/0000-0003-2203-9662; Email: ruijie.darius.teo@duke.edu

David N. Beratan − *Department of Chemistry and Department of Biochemistry, Duke University, Durham, North Carolina 27708, United States; Department of Physics, Duke University, Durham, North Carolina 27708, United States;* orcid.org/0000-0003-4758-8676; Email: david.beratan@duke.edu

Authors

Xiaochen Du − *Department of Chemistry, Duke University, Durham, North Carolina 27708, United States; Department of Computer Science, Duke University, Durham, North Carolina 27708, United States*

Héctor Luis Torres Vera − *Department of Molecular and Cell Biology, University of California, Berkeley, California 94720, United States*

Agostino Migliore − *Department of Chemistry, Duke University, Durham, North Carolina 27708, United States;* orcid.org/0000-0001-7780-2296

Complete contact information is available at: https://pubs.acs.org/10.1021/acs.jpcb.0c08598

Author Contributions

The manuscript was written through contributions of all authors.

Notes

The authors declare no competing financial interest.

ACKNOWLEDGMENTS

We thank Tomasz Janowski for technical support with the computing cluster at Duke University. This research is supported by the National Institutes of Health (grant GM-48043) and the Blue Waters sustained-petascale computing project (R.D.T.), which is funded by the National Science Foundation (Awards OCI-0725070 and ACI-1238993) and the State of Illinois.

REFERENCES

(1) Beratan, D. N.; Liu, C. R.; Migliore, A.; Polizzi, N. F.; Skourtis, S. S.; Zhang, P.; Zhang, Y. Q. Charge Transfer in Dynamical Biosystems, or the Treachery of (Static) Images. *Acc. Chem. Res.* **2015**, *48*, 474−481.

(2) Arnold, A. R.; Grodick, M. A.; Barton, J. K. DNA Charge Transport From Chemical Principles to the Cell. *Cell Chem. Biol.* **2016**, *23*, 183−197.

(3) Barton, J. K.; Silva, R. M. B.; O'Brien, E. Redox Chemistry in the Genome: Emergence of the [4Fe4S] Cofactor in Repair and Replication. *Annu. Rev. Biochem.* **2019**, *88*, 163−190.

(4) Boal, A. K.; Genereux, J. C.; Sontz, P. A.; Gralnick, J. A.; Newman, D. K.; Barton, J. K. Redox Signaling Between DNA Repair Proteins for Efficient Lesion Detection. *Proc. Natl. Acad. Sci. U. S. A.* **2009**, *106*, 15237−15242.

(5) Sato, R.; Kitoh-Nishioka, H.; Ando, K.; Yamato, T. Electron Transfer Pathways of Cyclobutane Pyrimidine Dimer Photolyase Revisited. *J. Phys. Chem. B* **2018**, *122*, 6912−6921.

(6) Grodick, M. A.; Segal, H. M.; Zwang, T. J.; Barton, J. K. DNA-Mediated Signaling by Proteins with 4Fe−4S Clusters is Necessary for Genomic Integrity. *J. Am. Chem. Soc.* **2014**, *136*, 6470−6478.

(7) O'Brien, E.; Holt, M. E.; Thompson, M. K.; Salay, L. E.; Ehlinger, A. C.; Chazin, W. J.; Barton, J. K. The [4Fe4S] Cluster of Human DNA Primase Functions as a Redox Switch Using DNA Charge Transport. *Science* **2017**, *355*, eaag1789.

(8) Teo, R. D.; Rousseau, B. J. G.; Smithwick, E. R.; Di Felice, R.; Beratan, D. N.; Migliore, A. Charge Transfer Between [4Fe4S] Proteins and DNA is Unidirectional. *Imp. for Biomol. Signaling. Chem* **2019**, *5*, 122−137.

(9) Beratan, D. N. Why are DNA and Protein Electron Transfer so Different? *Annu. Rev. Phys. Chem.* **2019**, *70*, 71−97.

(10) Slinker, J. D.; Muren, N. B.; Renfrew, S. E.; Barton, J. K. DNA Charge Transport Over 34 nm. *Nat. Chem.* **2011**, *3*, 228−233.

(11) Di Meo, S.; Reed, T. T.; Venditti, P.; Victor, V. M. Harmful and Beneficial Role of ROS. *Oxid. Med. Cell. Longevity* **2016**, *2016*, 1.

(12) Schieber, M.; Chandel, N. S. ROS Function in Redox Signaling and Oxidative Stress. *Curr. Biol.* **2014**, *24*, R453−R462.

(13) Yang, W. Y.; Zou, L. Z.; Huang, C. H.; Lei, Y. L. Redox Regulation of Cancer Metastasis: Molecular Signaling and Therapeutic Opportunities. *Drug Dev. Res.* **2014**, *75*, 331−341.

(14) Fuss, J. O.; Tsai, C.-L.; Ishida, J. P.; Tainer, J. A. Emerging Critical Roles of Fe−S Clusters in DNA Replication and Repair. *Biochim. Biophys. Acta-Mol. Cell Res.* **2015**, *1853*, 1253−1271.

(15) Johnson, D. C.; Dean, D. R.; Smith, A. D.; Johnson, M. K. Structure, Function, and Formation of Biological Iron-Sulfur Clusters. *Annu. Rev. Biochem.* **2005**, *74*, 247−281.

(16) Tse, E. C. M.; Zwang, T. J.; Barton, J. K. The Oxidation State of [4Fe4S] Clusters Modulates the DNA-Binding Affinity of DNA Repair Proteins. *J. Am. Chem. Soc.* **2017**, *139*, 12784−12792.

(17) Bartels, P. L.; Zhou, A.; Arnold, A. R.; Nuñez, N. N.; Crespilho, F. N.; David, S. S.; Barton, J. K. Electrochemistry of the [4Fe4S] Cluster in Base Excision Repair Proteins: Tuning the Redox Potential with DNA. *Langmuir* **2017**, *33*, 2523−2530.

(18) Gorodetsky, A. A.; Boal, A. K.; Barton, J. K. Direct Electrochemistry of Endonuclease III in the Presence and Absence of DNA. *J. Am. Chem. Soc.* **2006**, *128*, 12082−12083.

(19) Teo, R. D.; Wang, R.; Smithwick, E. R.; Migliore, A.; Therien, M. J.; Beratan, D. N. Mapping Hole Hopping Escape Routes in Proteins. *Proc. Natl. Acad. Sci. U. S. A.* **2019**, *116*, 15811−15816.

(20) Teo, R. D.; Migliore, A.; Beratan, D. N. Mutation Effects on Charge Transport Through the p58c Iron-Sulfur Protein. *Chem. Sci.* **2020**, *11*, 7076−7085.

(21) Boal, A. K.; Yavin, E.; Lukianova, O. A.; O'Shea, V. L.; David, S. S.; Barton, J. K. DNA-Bound Redox Activity of DNA Repair Glycosylases Containing [4Fe-4S] Clusters. *Biochemistry* **2005**, *44*, 8397−8407.

(22) Sontz, P. A.; Mui, T. P.; Fuss, J. O.; Tainer, J. A.; Barton, J. K. DNA Charge Transport as a First Step in Coordinating the Detection of Lesions by Repair Proteins. *Proc. Natl. Acad. Sci. U. S. A.* **2012**, *109*, 1856−1861.

(23) Fromme, J. C.; Banerjee, A.; Huang, S. J.; Verdine, G. L. Structural Basis for Removal of Adenine Mispaired with 8-Oxoguanine by MutY Adenine DNA Glycosylase. *Nature* **2004**, *427*, 652−656.

(24) Boon, E. M.; Pope, M. A.; Williams, S. D.; David, S. S.; Barton, J. K. DNA-Mediated Charge Transport as a Probe of MutY/DNA Interaction. *Biochemistry* **2002**, *41*, 8464−8470.

(25) Boon, E. M.; Livingston, A. L.; Chmiel, N. H.; David, S. S.; Barton, J. K. DNA-Mediated Charge Transport for DNA Repair. *Proc. Natl. Acad. Sci. U. S. A.* **2011**, *100*, 12543−12547.

(26) Lewis, F. D.; Young, R. M.; Wasielewski, M. R. Tracking Photoinduced Charge Separation in DNA: From Start to Finish. *Acc. Chem. Res.* **2018**, *51*, 1746−1754.

(27) Bai, H.; Grist, S.; Gardner, J.; Suthers, G.; Wilson, T. M.; Lu, A. L. Functional Characterization of Human MutY Homolog (hMYH) Missense Mutation (R231L) That is Linked With hMYH-Associated Polyposis. *Cancer Lett.* **2007**, *250*, 74−81.

(28) Šali, A.; Blundell, T. L. Comparative Protein Modelling by Satisfaction of Spatial Restraints. *J. Mol. Biol.* **1993**, *234*, 779−815.

(29) Schrödinger. *The PyMOL Molecular Graphics System, Version 2.1*; LLC.
(30) Lee, S.; Verdine, G. L. Atomic Substitution Reveals the Structural Basis for Substrate Adenine Recognition and Removal by Adenine DNA Glycosylase. *Proc. Natl. Acad. Sci. U. S. A.* **2009**, *106*, 18497−18502.
(31) Phillips, J. C.; Braun, R.; Wang, W.; Gumbart, J.; Tajkhorshid, E.; Villa, E.; Chipot, C.; Skeel, R. D.; Kalé, L.; Schulten, K. Scalable Molecular Dynamics with NAMD. *J. Comput. Chem.* **2005**, *26*, 1781−1802.
(32) Senftle, T. P.; Hong, S.; Islam, M. M.; Kylasa, S. B.; Zheng, Y. X.; Shin, Y. K.; Junkermeier, C.; Engel-Herbert, R.; Janik, M. J.; Aktulga, H. M.; et al. The ReaxFF Reactive Force-Field: Development, Applications and Future Directions. *npj Comput. Mater.* **2016**, *2*, 15011.
(33) Cheng, X.; Kelso, C.; Hornak, V.; de los Santos, C.; Grollman, A. P.; Simmerling, C. Dynamic Behavior of DNA Base Pairs Containing 8-Oxoguanine. *J. Am. Chem. Soc.* **2005**, *127*, 13906−13918.
(34) Maier, J. A.; Martinez, C.; Kasavajhala, K.; Wickstrom, L.; Hauser, K. E.; Simmerling, C. ff14SB: Improving the Accuracy of Protein Side Chain and Backbone Parameters from ff99SB. *J. Chem. Theory Comput.* **2015**, *11*, 3696−3713.
(35) Wang, J.; Cieplak, P.; Kollman, P. A. How Well Does a Restrained Electrostatic Potential (RESP) Model Perform in Calculating Conformational Energies of Organic and Biological Molecules? *J. Comput. Chem.* **2000**, *21*, 1049−1074.
(36) Pérez, A.; Marchán, I.; Svozil, D.; Sponer, J.; Cheatham, T. E.; Laughton, C. A.; Orozco, M. Refinement of the AMBER Force Field for Nucleic Acids: Improving the Description of α/γ Conformers. *Biophys. J.* **2007**, *92*, 3817−3829.
(37) Ryckaert, J.-P.; Ciccotti, G.; Berendsen, H. J. C. Numerical Integration of the Cartesian Equations of Motion of a System with Constraints: Molecular Dynamics of *n*-Alkanes. *J. Comput. Phys.* **1977**, *23*, 327−341.
(38) Darden, T.; York, D.; Pedersen, L. Particle Mesh Ewald: An $N\cdot\log(N)$ Method for Ewald Sums in Large Systems. *J. Chem. Phys.* **1993**, *98*, 10089−10092.
(39) Martyna, G. J.; Tobias, D. J.; Klein, M. L. Constant Pressure Molecular Dynamics Algorithms. *J. Chem. Phys.* **1994**, *101*, 4177−4189.
(40) Feller, S. E.; Zhang, Y. H.; Pastor, R. W.; Brooks, B. R. Constant Pressure Molecular-Dynamics Simulation: the Langevin Piston Method. *J. Chem. Phys.* **1995**, *103*, 4613−4621.
(41) Marcus, R. A.; Sutin, N. Electron Transfers in Chemistry and Biology. *Biochim. Biophys. Acta* **1985**, *811*, 265−322.
(42) Teo, R. D.; Smithwick, E. R.; Migliore, A. 2′-Deoxy-2′-Fluoro-Arabinonucleic Acid: A Valid Alternative to DNA for Biotechnological Applications Using Charge Transport. *Phys. Chem. Chem. Phys.* **2019**, *21*, 22869−22878.
(43) Teo, R. D.; Terai, K.; Migliore, A.; Beratan, D. N. Electron Transfer Characteristics of 2′-Deoxy-2′-Fluoro-Arabinonucleic Acid, a Nucleic Acid with Enhanced Chemical Stability. *Phys. Chem. Chem. Phys.* **2018**, *20*, 26063−26067.
(44) Oppenheim, I.; Shuler, K. E.; Weiss, G. H. Stochastic Theory of Nonlinear Rate Processes with Multiple Stationary States. *Phys. A* **1977**, *88*, 191−214.
(45) Procaccia, I.; Mukamel, S.; Ross, J. On the Theory of Unimolecular Reactions: Application of Mean First Passage Time to Reaction Rates. *J. Chem. Phys.* **1978**, *68*, 3244−3253.
(46) Bar-Haim, A.; Klafter, J. On Mean Residence and First Passage Times in Finite One-Dimensional Systems. *J. Chem. Phys.* **1998**, *109*, 5187−5193.
(47) Steenken, S.; Jovanovic, S. V. How Easily Oxidizable is DNA? One-Electron Reduction Potentials of Adenosine and Guanosine Radicals in Aqueous Solution. *J. Am. Chem. Soc.* **1997**, *119*, 617−618.
(48) Banyasz, A.; Ketola, T.-M.; Muñoz-Losa, A.; Rishi, S.; Adhikary, A.; Sevilla, M. D.; Martinez-Fernandez, L.; Improta, R.; Markovitsi, D. UV-Induced Adenine Radicals Induced in DNA A-Tracts: Spectral and Dynamical Characterization. *J. Phys. Chem. Lett.* **2016**, *7*, 3949−3953.
(49) Prindle, M. J.; Loeb, L. A. DNA Polymerase Delta in DNA Replication and Genome Maintenance. *Environ. Mol. Mutagen.* **2012**, *53*, 666−682.

https://dx.doi.org/10.1021/acs.jpcb.0c08598
J. Phys. Chem. B 2021, 125, 17−23